Symmetries and triplet dispersion in a modified Shastry-Sutherland model for $SrCu_2(BO_3)_2$

2000 J. Phys.: Condens. Matter 12 9069

(http://iopscience.iop.org/0953-8984/12/42/312)

J. Phys.: Condens. Matter **12** (2000) 9069–9083. Printed in the UK PII: S0953-8984(00)16456-2

Symmetries and triplet dispersion in a modified Shastry–Sutherland model for $SrCu_2(BO_3)_2$

Christian Knetter†, Erwin Müller-Hartmann and Götz S Uhrig‡

Institut für Theoretische Physik, Universität zu Köln, Zülpicher Strasse 77, D-50937 Köln, Germany

E-mail: ck@thp.uni-koeln.de (C Knetter) and gu@thp.uni-koeln.de (G S Uhrig)

Received 17 August 2000

Abstract. We investigate the one-triplet dispersion in a modified Shastry–Sutherland model for $SrCu_2(BO_3)_2$ by means of a series expansion about the limit of strong dimerization. Our perturbative method is based on a continuous unitary transformation that maps the original Hamiltonian to an effective, energy-quanta-conserving block diagonal Hamiltonian $\mathcal{H}_{\text{eff}}$. The dispersion splits into two branches which are nearly degenerate. We analyse the symmetries of the model and show that space group operations are necessary to explain the degeneracy of the dispersion at $\boldsymbol{k} = \boldsymbol{0}$ and at the border of the magnetic Brillouin zone. Moreover, we investigate the behaviour of the dispersion for small $|\boldsymbol{k}|$ and compare our results to inelastic neutron scattering data.

1. Introduction

The study of quantum spin systems exhibiting a finite spin gap has advanced significantly through the recent synthesis of novel magnetic materials. While quasi-one-dimensional systems have been studied for a long time now, new interest arose from the discovery of new quasi-two-dimensional materials like CaV_4O_9 [1] and $(VO_2)P_2O_7$ [2]. Particularly interesting is $SrCu_2(BO_3)_2$ [3], since it is an experimental realization of the Shastry–Sutherland model [4, 5]. In reference [6] we presented an extended version of that model (figure 1) and deduced its $T = 0$ phase diagram in the model parameter space.

The Hamiltonian is given by

$$H = \underbrace{J_1 \sum_{\langle i,j \rangle} \vec{S}_i \cdot \vec{S}_j}_{H_0} + \underbrace{J_2 \sum_{\langle i,k \rangle} \vec{S}_i \cdot \vec{S}_k}_{H_1} + \underbrace{J_3 \sum_{\langle i,l \rangle} \vec{S}_i \cdot \vec{S}_l}_{H_2} \tag{1}$$

where the bonds corresponding to interactions J_1, J_2 and J_3 are shown in figure 1. For $J_3 = 0$ the model reduces to the original Shastry–Sutherland model.

It can be easily verified that the singlet–dimer state (singlets on all strong bonds J_1, henceforth called dimers) is an exact eigenstate of our model: a single spin interacts via J_2 and J_3 with $S = 0$ objects only. Thus the corresponding terms in Hamiltonian (1) do not contribute. The remaining expression simply gives $-(3/8)J_1$ per spin. This article focuses on the region where the singlet–dimer state is the ground state, called the dimer phase. In this phase a single excitation (magnon) is introduced by breaking up one singlet and substituting

† Internet: www.thp.uni-koeln.de/~ck/.
‡ Internet: www.thp.uni-koeln.de/~gu/.

0953-8984/00/429069+15$30.00

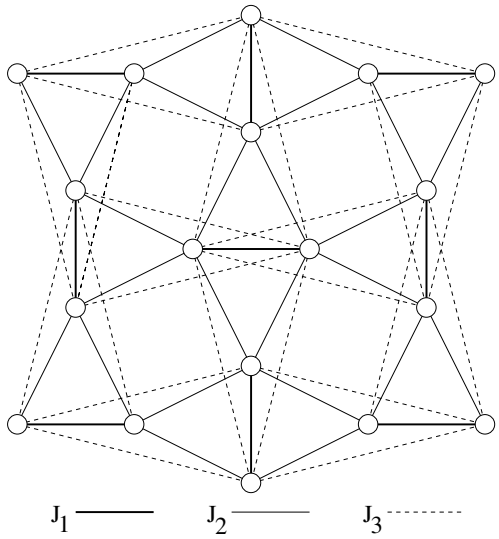

Figure 1. A portion of the lattice that we suggest for $SrCu_2(BO_3)_2$. The coupling J_1 is assumed to be antiferromagnetic. The starting point of our analysis is the limit of strong dimerization ($J_2, J_3 \to 0$).

one triplet instead (the triplet's z-component is irrelevant). By hopping from dimer to dimer this triplet acquires a dispersion, which we intend to calculate. It suffices to do the calculations on an effective square lattice Γ_{eff}, where one site represents one dimer. Note that Γ_{eff} has a sublattice structure A/B, where A (B) corresponds to vertical (horizontal) dimers.

We derive a power series expansion about the limit of strong dimerization ($J_2, J_3 \to 0$) for the one-magnon dispersion. By fitting the expansion to INS data obtained by Kageyama *et al* [7] we deduce model parameters which show good agreement with parameters previously determined [8].

The next section gives a short introduction to the method used. Before we calculate and discuss the one-magnon dispersion (section 4) we use some of the model's symmetries to derive interesting and useful relations between various hopping amplitudes (section 3).

2. Method and qualitative pictures

The one-magnon dispersion is calculated perturbatively about the limit of isolated dimers using the flow equation method introduced previously [9]. Given a perturbation problem that can be formulated in the standard way:

$$\mathcal{H} = \mathcal{H}_0 + x\mathcal{H}_S \tag{2}$$

this method in its present formulation relies only on two further prerequisites:

(A) The unperturbed Hamiltonian $\mathcal{H}_0$ must have an equidistant spectrum bounded from below. The difference between two successive levels is called an energy quantum.

(B) There is a number $\mathbb{N} \ni N > 0$ such that the perturbing Hamiltonian H_S can be written as $H_S = \sum_{n=-N}^{N} T_n$ where T_n increments (or decrements, if $n < 0$) the number of energy quanta by n.

The flow equation method maps the perturbed Hamiltonian $\mathcal{H}$ by a continuous unitary transformation to an effective Hamiltonian $\mathcal{H}_{\text{eff}}$, which *conserves* the number of energy quanta, i.e. $[\mathcal{H}_{\text{eff}}, \mathcal{H}_0] = 0$. Thus the effective Hamiltonian is block diagonal and has the form

$$\mathcal{H}_{\text{eff}} = \mathcal{H}_0 + \sum_{k=1}^{\infty} x^k \sum_{|\underline{m}|=k, M(\underline{m})=0} C(\underline{m}) T(\underline{m}) \tag{3}$$

where $\underline{m}$ is a vector of dimension k whose components are in $\{\pm N, \pm(N-1), \ldots \pm 1, 0\}$; $M(\underline{m}) = 0$ signifies that the sum of the components vanishes, which reflects the conservation of the number of energy quanta. The operator product $T(\underline{m})$ is defined by $T_{\underline{m}} = T_{m_1} T_{m_2} \cdots T_{m_k}$, where k is the order of the process. The coefficients $C(\underline{m})$ are generally valid fractions, which we computed up to order $k = 15$ for $N = 1$ and up to order $k = 10$ for $N = 2$ (cf. reference [9]).

We want to emphasize that the effective Hamiltonian $\mathcal{H}_{\text{eff}}$ with known coefficients $C(\underline{m})$ can be used straightforwardly in all perturbative problems that meet conditions (A) and (B). The interested reader can find the $C(\underline{m})$ and additional information on our homepages. For checking purposes we tested the $C(\underline{m})$ by applying the method to toy models. In the $N = 1$ case, for instance, we considered the one-dimensional harmonic oscillator perturbed by itself and an additional linear potential. Thus, with $\hbar\omega = 1$,

$$\mathcal{H}_0 = \frac{1}{2}(P^2 + X^2) = a^\dagger a + \frac{1}{2} \tag{4}$$

$$\mathcal{H}_S = \frac{1}{2}(P^2 + X^2) + X = \underbrace{a^\dagger a + \frac{1}{2}}_{T_0} + \underbrace{\frac{1}{\sqrt{2}} a^\dagger}_{T_1} + \underbrace{\frac{1}{\sqrt{2}} a}_{T_{-1}}. \tag{5}$$

In this case equation (2) can be solved exactly to give

$$E_n = (1+x)\left(n + \frac{1}{2}\right) - \frac{1}{2}\frac{x^2}{1+x}. \tag{6}$$

We expand this last equation about $x = 0$ and obtain

$$E_n = n + \frac{1}{2} + \frac{1}{2}(2n+1)x - \frac{1}{2}\sum_{i=2}^{\infty}(-1)^i x^i. \tag{7}$$

By inserting the T_i defined in equation (5) in the effective Hamiltonian (3) and calculating $\langle n|\mathcal{H}_{\text{eff}}|n\rangle$ with $n \in \mathbb{N}$ we retain equation (7) exactly up to 15th order.

We now show that Hamiltonian (1) meets conditions (A) and (B) for $N = 1$. To this end we rewrite equation (1):

$$\frac{H}{J_1} = H_0 + x H_S \tag{8}$$

with

$$H_S = H_1 + \frac{y}{x} H_2 \qquad x = \frac{J_2}{J_1} \qquad y = \frac{J_3}{J_1}. \tag{9}$$

In the limit of isolated dimers ($x = 0$, with y/x finite), H is bounded from below and has an equidistant energy spectrum since up to a trivial constant H_0 simply counts the number of excited dimers, i.e. energy quanta.

To decompose H_S we follow the same procedure as in reference [9] and state the result:

$$H_S = T_{-1} + T_0 + T_1 \tag{10}$$

with

$$T_{\pm 1} = \frac{1}{2}\left(1 - \frac{y}{x}\right)\sum_{\nu} \mathcal{T}_{\pm 1}(\nu) \tag{11}$$

$$T_0 = \frac{1}{2}\left(1 + \frac{y}{x}\right)\sum_{\nu} \mathcal{T}_0(\nu) \tag{12}$$

where ν denotes the pairs of adjacent dimers. For some fixed ν we encounter the pair depicted in figure 2, the state of which is determined by $|x_1, x_2\rangle$, where $x_1, x_2 \in \{s, t^1, t^0, t^{-1}\}$ are singlets or one of the triplets occupying the vertical (horizontal) dimer, respectively. The superscript $n \in \{0, \pm 1\}$ in t^n stands for the S^z-component. For the pair $|x_1, x_2\rangle$ we give the action of the local operators $\mathcal{T}_i$ in table 1.

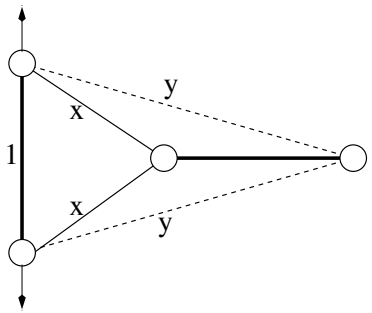

Figure 2. A pair of adjacent dimers (intra-dimer coupling constant set to unity) connected by the perturbing interactions x and y. The local operators $\mathcal{T}_i$ as defined in table 1 acquire a global minus, if we reflect the pair on the axis indicated and keep the notation $|x_1, x_2\rangle$ as defined in the text. This is due to the singlet antisymmetry under reflection.

Table 1. The action of the local operators $\mathcal{T}_0$ and $\mathcal{T}_1$ as they appear in equations (11), (12) on all relevant states of the dimer pair depicted in figure 2. These operators conserve the total S^z-component. Note that $\mathcal{T}_1$ can only create another triplet on the horizontal dimer if one already exists on the vertical dimer. This has also been noticed in reference [10]. Possible $\mathcal{T}_{\pm 2}$-operators cancel out due to the inherent frustration of the lattice. Matrix elements not listed are zero.

$\mathcal{T}_0$		
$\|t^{\pm 1}, t^{\pm 1}\rangle$	$\longrightarrow$	$\|t^{\pm 1}, t^{\pm 1}\rangle$
$\|t^{\pm 1}, t^{0}\rangle$	$\longrightarrow$	$\|t^{0}, t^{\pm 1}\rangle$
$\|t^{\pm 1}, t^{\mp 1}\rangle$	$\longrightarrow$	$\|t^{0}, t^{0}\rangle - \|t^{\pm 1}, t^{\mp 1}\rangle$
$\|t^{0}, t^{0}\rangle$	$\longrightarrow$	$\|t^{1}, t^{-1}\rangle + \|t^{-1}, t^{1}\rangle$
$\|t^{0}, t^{\pm 1}\rangle$	$\longrightarrow$	$\|t^{\pm 1}, t^{0}\rangle$
$\mathcal{T}_1$		
$\|t^{\pm 1}, s\rangle$	$\longrightarrow$	$\mp\|t^{0}, t^{\pm 1}\rangle \pm \|t^{\pm 1}, t^{0}\rangle$
$\|t^{0}, s\rangle$	$\longrightarrow$	$\|t^{1}, t^{-1}\rangle - \|t^{-1}, t^{1}\rangle$

The remaining matrix elements can be constructed by using $\mathcal{T}_n^\dagger = \mathcal{T}_{-n}$. Note that we need to fix the orientation for singlets, say spin up with positive sign always at the right-hand (upper) site of the dimers. Hence $\mathcal{T}_1$ and $\mathcal{T}_{-1}$ acquire a global minus for oppositely oriented dimer pairs (reflection of the dimer pair in figure 2 about the vertical dimer).

Instead of Hamiltonian (1) we can now use the effective Hamiltonian $\mathcal{H}_{\text{eff}}$ (equation (3)) with the T_i defined in equations (11), (12). The effective Hamiltonian (3) simplifies the computations considerably. Since $[\mathcal{H}_{\text{eff}}, \mathcal{H}_0] = 0$, $\mathcal{H}_{\text{eff}}$ is block diagonal allowing triplet-conserving processes only. Thus the effective Hamiltonian acts in a much smaller Hilbert space than the original problem, which is a great advantage in the numerical implementation.

In addition to this simplification, the explicit form of $\mathcal{H}_{\text{eff}}$ provides a simple and comprehensive picture of the physics involved. Imagine we were to put a triplet on one of the dimers in the lattice. In the real substance this local excitation would polarize its environment due to the exchange couplings and must be viewed as a dressed quasi-particle surrounded by a cloud of virtual excitations fluctuating in space and time. The effective Hamiltonian includes these fluctuations as virtual processes $T(\underline{m})$, each weighted by the factor $C(\underline{m})$. Each process ends with a state having the same number of triplets as the initial state. Other quantum numbers such as the total spin are also conserved. As the order k is increased, more and longer processes are allowed for and the accuracy of the results will be enhanced. Inspecting the weight factors $C(\underline{m})$ shows that longer processes have less influence.

Let us follow one of the possible virtual processes and understand why the observed triplet dispersion of $SrCu_2(BO_3)_2$ is rather flat (cf. figure 8, later). Suppose we begin with one triplet in the lattice as depicted in the upper left-hand corner of figure 3.

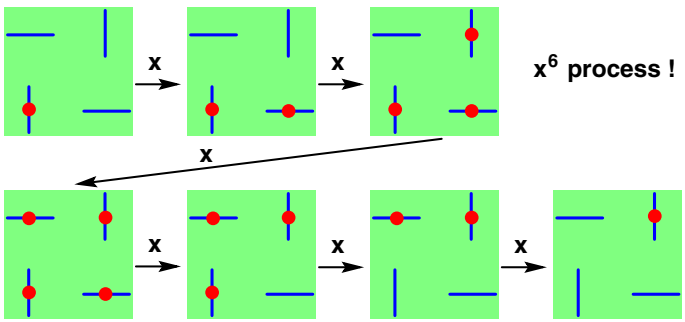

Figure 3. The leading (virtual) process for one-triplet hopping corresponding to $x^6 T(\underline{m}) = x^6 T_{-1} T_{-1} T_{-1} T_1 T_1 T_1$. Dark dots are triplets, bars are dimers. There is no lower-order process leading to one-triplet motion.

By applying T_1 once we can create another triplet only on one of the two *horizontally* adjacent dimers as is clear from table 1 and figure 2. From there we might create another one and so on until we can close a circle (bottom left-hand state in figure 3). We now start destroying triplets by T_{-1}-processes and end up with the shifted triplet. The amplitude for this hopping is $\propto x^6$. It is the largest amplitude that one can find (see also reference [10]). Therefore the triplets are rather localized, leading to a flat dispersion.

Note that the T_1-processes (T_{-1}-processes) are proportional to $(x - y)$ (see equation (11)). So, the leading triplet motion is $\mathcal{O}((x - y)^6)$ in leading order. Even local processes (without hopping) include at least two T_1-processes (T_{-1}-processes). Hence all perturbative amplitudes are at least of order $(x - y)^2$. We will make use of this fact later on.

Examining the two-triplet sector [8] we showed that *correlated* hopping processes occur in second order already. The actual dispersion, however, sets in only in third order. This much lower order (x^3 instead of x^6) explains the much stronger two-magnon dispersion [7].

To quantify the picture constructed let $|\boldsymbol{r}\rangle = |r_1, r_2\rangle$ denote the state of the system with one triplet at $\boldsymbol{r} \in \Gamma_{\text{eff}}$ and singlets on all other sites. The amplitude $t^{o(r)}_{\boldsymbol{r}'-\boldsymbol{r}}$ for a triplet hopping

from site $\boldsymbol{r}$ to site $\boldsymbol{r}'$ is given by

$$t_{\boldsymbol{r}'-\boldsymbol{r}}^{o(\boldsymbol{r})} = \langle \boldsymbol{r}' | \mathcal{H}_{\text{eff}} | \boldsymbol{r} \rangle \tag{13}$$

where the upper index $o(\boldsymbol{r}) \in \{v, h\}$ allows one to distinguish whether the hopping started on a vertically oriented (v) or a horizontally oriented dimer (h). Furthermore we choose to split the hopping amplitudes into an average part $\bar{t}_s$ and an alternating part $\mathrm{d}t_s$ ($\boldsymbol{s} = \boldsymbol{r}' - \boldsymbol{r}$):

$$t_{\boldsymbol{s}}^{o(\boldsymbol{r})} = \bar{t}_s + \mathrm{e}^{\mathrm{i}\boldsymbol{Q}\cdot\boldsymbol{r}}\, \mathrm{d}t_s \tag{14}$$

with $\boldsymbol{Q} = (\pi, \pi)$.

The right-hand side of equation (13) can be easily implemented on a computer. For details see reference [9]. We want to point out, however, that all computations are done symbolically, i.e. we obtain results as functions (polynomials) of all model parameters.

3. Symmetries

Before we calculate the one-triplet dispersion quantitatively in the next section, it is worthwhile to look at the symmetries that the model in figure 1 displays. The two-dimensional space group of the model can be identified to be $p4mm$ with the underlying point group $4mm$ as can be verified in figure 4.

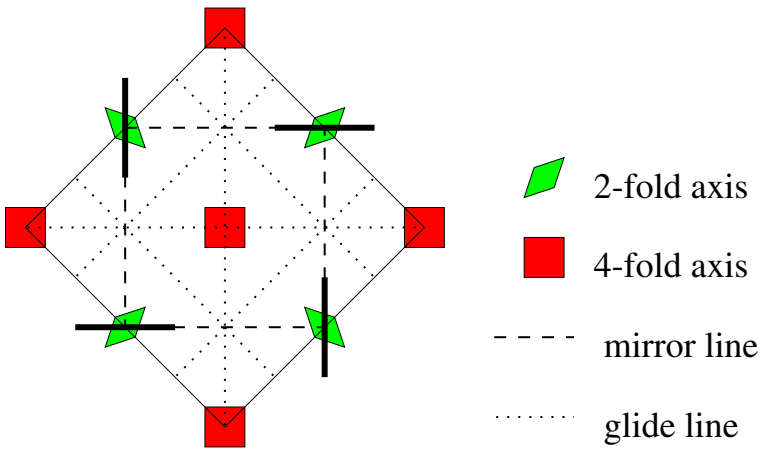

Figure 4. A possible unit cell of the Shastry–Sutherland model with the dimers arranged at the sides of the cell. All symmetries are depicted. The two-dimensional crystallographic space group is $p4mm$.

We will not treat all symmetry aspects but concentrate on those that will be of use later on. We choose the coordinate system parallel to the dimers such that one dimer (horizontal or vertical) lies in the origin and introduce two diagonals u and v crossing the origin with slope -1 and 1, respectively. The distance between the centres of two adjacent dimers is set to unity.

Several relations between different hopping amplitudes can be deduced. To this end we define six symmetry operations which map the lattice onto itself. Note that the fixed singlet orientation can lead to negative phase factors.

- $m_{x/y}$: reflection about the x/y-axis:

$$m_{x/y}|r_1, r_2\rangle = (-1)^{r_1+r_2}|\pm r_1, \mp r_2\rangle.$$

- I: inversion about the origin:

$$I|r_1, r_2\rangle = |-r_1, -r_2\rangle.$$

- $\sigma_{v/u}$: reflection about the diagonals v/u plus translation by $(0, -1)$:

$$\sigma_{v/u}|r_1, r_2\rangle = |\pm r_2, \pm r_1 - 1\rangle.$$

- R: rotation of $\pi/2$ about the origin plus translation by $(0, -1)$:

$$R|r_1, r_2\rangle = (-1)^{r_1+r_2}|-r_2, r_1 - 1\rangle.$$

Since these operations leave $\mathcal{H}$ unchanged they all commute with $\mathcal{H}_{\text{eff}}$. Applying m_x to equation (13) we find

$$\begin{aligned} t^{o(\boldsymbol{r})}_{\boldsymbol{r}'-\boldsymbol{r}} &= (-1)^{r_1'+r_2'}\langle r_1', -r_2'|m_x\mathcal{H}_{\text{eff}}|r_1, r_2\rangle = (-1)^{r_1+r_2+r_1'+r_2'}\langle r_1', -r_2'|\mathcal{H}_{\text{eff}}|r_1, -r_2\rangle \\ &= (-1)^{r_1+r_2+r_1'+r_2'}t^{o(\boldsymbol{r})}_{(r_1', -r_2')-(r_1, -r_2)} \end{aligned} \tag{15}$$

or simply

$$t^{o(\boldsymbol{r})}_{\boldsymbol{s}} = (-1)^{s_1+s_2}t^{o(\boldsymbol{r})}_{s_1, -s_2}. \tag{16}$$

Analogously using m_y, I, σ_u, σ_v and R we find

$$t^{o(\boldsymbol{r})}_{\boldsymbol{s}} = (-1)^{s_1+s_2}t^{o(\boldsymbol{r})}_{-s_1, s_2} \tag{17}$$

$$= t^{o(\boldsymbol{r})}_{-\boldsymbol{s}} \tag{18}$$

$$= t^{o(\boldsymbol{r}-(0,1))}_{-s_2, -s_1} \tag{19}$$

$$= t^{o(\boldsymbol{r}-(0,1))}_{s_2, s_1} \tag{20}$$

$$= (-1)^{s_1+s_2}t^{o(\boldsymbol{r}-(0,1))}_{-s_2, s_1} \tag{21}$$

respectively. In particular equations (17) and (18) yield together

$$t^{o(\boldsymbol{r})}_{(-s_1,0)} = (-1)^{s1}t^{o(\boldsymbol{r})}_{(s1,0)} = t^{o(\boldsymbol{r})}_{(s1,0)} \Rightarrow t^{o(\boldsymbol{r})}_{(s_1,0)} = 0 \qquad \text{if } s_1 \text{ is odd} \tag{22}$$

and analogously

$$t^{o(\boldsymbol{r})}_{(-s_1,0)} = (-1)^{s1}t^{o(\boldsymbol{r})}_{(s1,0)} = t^{o(\boldsymbol{r})}_{(s1,0)} \Rightarrow t^{o(\boldsymbol{r})}_{(0,s_2)} = 0 \qquad \text{if } s_2 \text{ is odd} \tag{23}$$

describing the interesting fact that hopping along the axis has non-zero amplitude only if this hopping moves the triplet an even number of sites (Γ_{eff}).

4. Dispersion

Since $\mathcal{H}_{\text{eff}}$ conserves the number of triplets, the one-triplet dispersion is particularly easy to calculate. Starting with one triplet this excitation can only be shifted, i.e. the triplet hops on the effective lattice Γ_{eff}. Additional care has to be taken to account for the sublattice structure of Γ_{eff}. From equation (13) we get

$$\mathcal{H}_{\text{eff}}|\boldsymbol{r}\rangle = \sum_{\boldsymbol{r}}{}' t^{o(\boldsymbol{r})}_{\boldsymbol{r}'}|\boldsymbol{r} + \boldsymbol{r}'\rangle. \tag{24}$$

We introduce Fourier-transformed states:

$$|\sigma, \boldsymbol{k}\rangle = \frac{1}{\sqrt{L}}\sum_{\boldsymbol{r}}|\boldsymbol{r}\rangle e^{i(\boldsymbol{k}+\sigma\boldsymbol{Q})\cdot\boldsymbol{r}} \tag{25}$$

with the number of dimers L, the new quantum number $\sigma \in \{0, 1\}$ reflecting the sublattice structure and $\boldsymbol{k}$ a vector in the magnetic Brillouin zone (MBZ). Calculating the action of $\mathcal{H}_{\text{eff}}|\sigma, \boldsymbol{k}\rangle$ on these states yields

$$\begin{aligned}\mathcal{H}_{\text{eff}}|\sigma, \boldsymbol{k}\rangle &= \frac{1}{\sqrt{L}} \sum_{r,r'} (\bar{t}_{r'} + \mathrm{e}^{\mathrm{i}\boldsymbol{Q}\cdot\boldsymbol{r}}\, \mathrm{d}t'_{\boldsymbol{r}}) |\boldsymbol{r} + \boldsymbol{r}'\rangle \mathrm{e}^{\mathrm{i}(\boldsymbol{k}+\sigma\boldsymbol{Q})\cdot\boldsymbol{r}} \\ &= \sum_{\boldsymbol{r}}{}' \bar{t}_{\boldsymbol{r}'} \mathrm{e}^{-\mathrm{i}(\boldsymbol{k}+\sigma\boldsymbol{Q})\cdot\boldsymbol{r}'} \underbrace{\frac{1}{\sqrt{L}} \sum_{\boldsymbol{r}} |\boldsymbol{r}\rangle \mathrm{e}^{\mathrm{i}(\boldsymbol{k}+\sigma\boldsymbol{Q})\cdot\boldsymbol{r}}}_{|\sigma,\boldsymbol{k}\rangle} \\ &\quad + \sum_{\boldsymbol{r}}{}' \mathrm{d}t_{\boldsymbol{r}'}\, \mathrm{e}^{-\mathrm{i}(\boldsymbol{k}+\bar{\sigma}\boldsymbol{Q})\cdot\boldsymbol{r}'} \underbrace{\frac{1}{\sqrt{L}} \sum_{\boldsymbol{r}} |\boldsymbol{r} + \boldsymbol{r}'\rangle \mathrm{e}^{\mathrm{i}(\boldsymbol{k}+\bar{\sigma}\boldsymbol{Q})\cdot(\boldsymbol{r}+\boldsymbol{r}')}}_{|\bar{\sigma},\boldsymbol{k}\rangle} \end{aligned} \tag{26}$$

with $\bar{\sigma} = 1 - \sigma$. We used the definitions (13) and (14). Further, since equation (18) holds for even and odd $r_1 + r_2$, one has $\bar{t}_s = \bar{t}_{-s}$ and $\mathrm{d}t_s = \mathrm{d}t_{-s}$. Thus we can simplify the sums over $\boldsymbol{r}'$ in equation (26) to give

$$\begin{aligned}\mathcal{H}_{\text{eff}}|\sigma, \boldsymbol{k}\rangle &= \underbrace{\left[\bar{t}_{\boldsymbol{0}} + 2 \sum_{\boldsymbol{r}>0} \bar{t}_{\boldsymbol{r}} \cos((\boldsymbol{k} + \sigma\boldsymbol{Q}) \cdot \boldsymbol{r})\right]}_{a_\sigma} |\sigma, \boldsymbol{k}\rangle \\ &\quad + \underbrace{\left[\mathrm{d}t_{\boldsymbol{0}} + 2 \sum_{\boldsymbol{r}>0} \mathrm{d}t_{\boldsymbol{r}} \cos((\boldsymbol{k} + \bar{\sigma}\boldsymbol{Q}) \cdot \boldsymbol{r})\right]}_{b} |\bar{\sigma}, \boldsymbol{k}\rangle \end{aligned} \tag{27}$$

with $\boldsymbol{r} > 0$ if and only if ($r_1 > 0$ or $r_1 = 0$ but $r_2 > 0$). In appendix A we show that $\mathrm{d}t_{\boldsymbol{0}} = 0$ and $\mathrm{d}t_{\boldsymbol{r}} = 0$ for $r_1 + r_2$ odd. Hence b does not depend on $\bar{\sigma}$:

$$b = 2 \sum_{\substack{\boldsymbol{r}>0 \\ r_1+r_2 \text{ even}}} \mathrm{d}t_{\boldsymbol{r}} \cos(\boldsymbol{k} \cdot \boldsymbol{r}) \tag{28}$$

and $\mathcal{H}_{\text{eff}}$ is symmetric in the new states. The remaining 2×2 problem can be solved easily to give the dispersion:

$$\omega_{1/2}(\boldsymbol{k}) = \underbrace{\frac{a_0 + a_1}{2}}_{\omega_0(\boldsymbol{k})} \pm \frac{1}{2}\sqrt{(a_0 - a_1)^2 + 4b^2}. \tag{29}$$

Thus the one-triplet dispersion splits into two branches. We want to point out, however, that at $\boldsymbol{k} = \boldsymbol{0}$ and at the borders of the MBZ (i.e. $|k_x + k_y| = \pi$ or $|k_y - k_x| = \pi$) the two branches fall onto each other leading to a twofold-degenerate dispersion. An analogous degeneracy is noticed in the two-triplet sector [8]. In appendix B we demonstrate that the degeneracy is due to the glide line symmetries R and $\sigma_{u/v}$ and show that $(a_0 - a_1)$ and b both vanish. Moreover, $(a_0 + a_1)$ is a sum over $\boldsymbol{r}$ with $r_1 + r_2$ even and thus contains 'even' hopping amplitudes only. At $\boldsymbol{k} = \boldsymbol{0}$ and at the border of the MBZ we therefore find that one-triplet hopping takes place on one species of the two sublattices A/B in Γ_{eff} only. In other words, the triplets live either on the horizontal or on the vertical dimers.

We calculated the amplitudes $\bar{t}_{\boldsymbol{r}}$ and $\mathrm{d}t_{\boldsymbol{r}}$ (and therefore the dispersion) as exact polynomials in x and y up to and including 15th order. On appearance of this article these polynomials will be published in electronic form on our homepages.

Expanding the square root in equation (29) about the limit of vanishing x and y produces terms $\propto x^\alpha y^\beta$ with $\alpha + \beta \geqslant 10$. Hence the energy splitting starts in the tenth order and is

negligible for all reasonable values of x and y. The fact that the splitting starts four orders later than the dispersion may be understood by observing that $(a_0 - a_1)$ is a sum over $\boldsymbol{r}$ with $r_1 + r_2$ odd. From the discussion at the end of section 3 it is clear that $t^{o(\boldsymbol{r})}_{\pm 1,0}$ and $t^{o(\boldsymbol{r})}_{0,\pm 1}$ vanish, with the result that the leading 'odd' process is $t^{o(r)}_{\pm 2,\pm 1}$ or $t^{o(r)}_{\pm 1,\pm 2}$, which start in tenth order only. One may object that b contains $\mathrm{d}t_{1,1}$, which could be larger, but from relation (A.5) in appendix A it follows that $\mathrm{d}t_{1,1} = 0$. The amplitudes $\mathrm{d}t_{\pm 2,0}$ and $\mathrm{d}t_{0,\pm 2}$ in b also start in tenth order only. Hence the near degeneracy in the one-triplet sector can be understood on the basis of the symmetries of the lattice.

By substituting $y = 0$ in $\omega_0(\boldsymbol{k})$ we obtain the decimal numbers computed by Zheng *et al* [11]. Our series expansion for the dispersion (29) converges nicely but it can be improved further by the use of D–log Padé approximants [12].

Let us first consider the energy gap $\Delta := \omega(0, 0)$ as a function of x and y. We fix the ratio of x and y and use D–log Padé approximants to extrapolate the remaining expression. For all x/y ratios that we tested, we find the approximants to be very stable, i.e. most of the possible approximants at a fixed ratio coincide very well. (Some are defective, i.e. they show spurious singularities.) Figure 5 shows D–log Padé extrapolations for $y = -x\tan(\pi/6)$ and $y = -x\tan(\pi/8)$. In reference [6] we used this technique to determine the line in the (x, y) plane where the gap Δ vanishes. The vanishing of Δ indicates definitively the breakdown of the dimer phase. But it may happen that another excitation becomes soft before the elementary triplet vanishes (cf. reference [8]) or that a first-order transition takes place [8, 13]. In the present work we choose to examine the elementary triplet only.

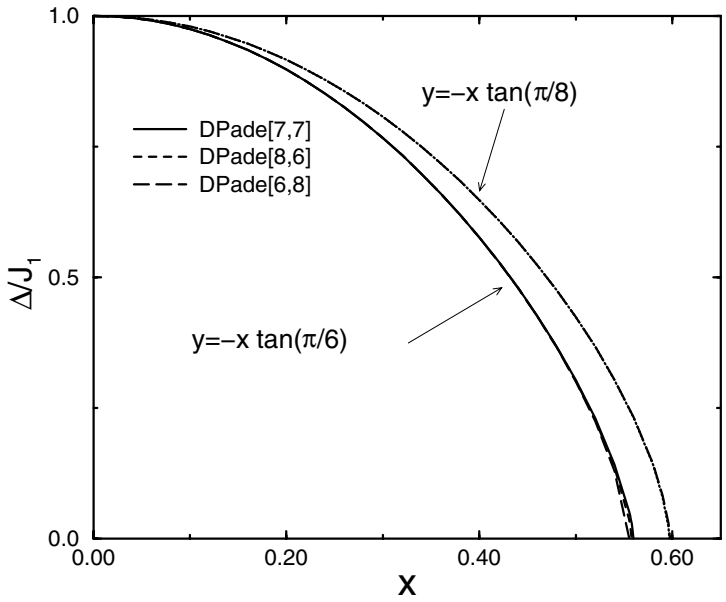

Figure 5. D–log Padé extrapolations of the gap along two lines in the (x, y) plane. Different approximants for a fixed ratio coincide very well. The (x, y) values where the gap vanishes constitute a line in the (x, y) plane indicating the definitive collapse of the dimer phase (cf. figure 2 in reference [6]).

For $y = -x\tan(\pi/6)$ the gap vanishes at $x = 0.558(1)$ ($y = -0.323(1)$). At this point we get the lowest curve in figure 6 where we choose to show the dispersion along a triangle in the MBZ.

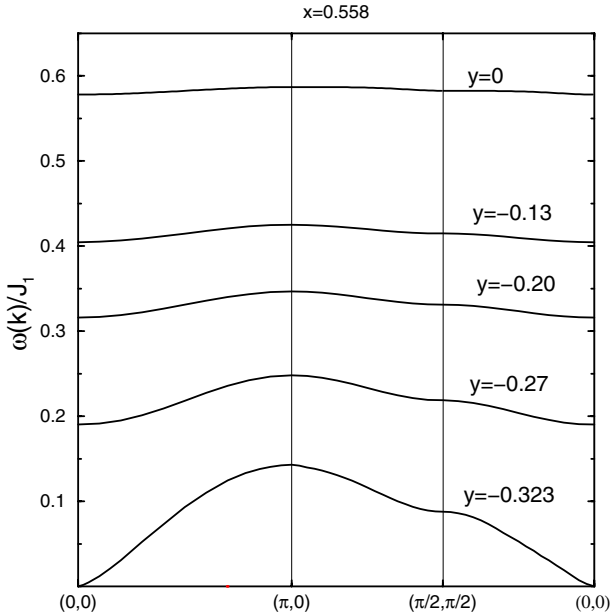

Figure 6. One-triplet dispersion in the MBZ at various points of the (x, y) plane. The lowest curve shows $\omega(\boldsymbol{k})$ at the point where the gap vanishes. With increasing y the dispersion decreases considerably, as is clear from $(\omega(\pi, 0) - \omega(0, 0)) \propto (x - y)^6$.

In section 2 we saw that all hopping amplitudes are proportional to $(x - y)^6$. Since the dispersion is a sum over these amplitudes it is clear that $(\omega(\pi, 0) - \omega(0, 0)) \propto (x - y)^6$. Indeed, for increasing y we see that the dispersion decreases (figure 6). At $x = y$ we find the dispersion to be absolutely flat. This is a signature of the fact that at $x = y$ the total spin on each J_1-bond is a conserved quantity [6]. Thus there will be no triplet motion.

We turn to the behaviour of the dispersion $\omega(\boldsymbol{k})$ for small $|\boldsymbol{k}|$ on the line in the (x, y) plane where the gap vanishes. After fixing the ratio x/y in equation (29) and applying the D–log Padé technique we end up with an expression

$$\omega(x; \boldsymbol{k}) = \exp\left[\int_0^x \underbrace{A(\boldsymbol{k})\frac{P(x; \boldsymbol{k})}{Q(x; \boldsymbol{k})}}_{f(x;\boldsymbol{k})}\right] \mathrm{d}x \tag{30}$$

where A is a function of $\boldsymbol{k}$ and P and Q are polynomials in x (where the leading coefficient is unity) of order M and N, respectively (shorthand: $[M, N]$ approximant). At $\boldsymbol{k} = 0$ the smallest positive zero of Q, say x_0, is the point where the exponent diverges logarithmically to $-\infty$; hence $\omega(x_0; 0) = 0$. We set $k_y = 0$ and will show that for small k_x

$$\omega(x_0; k_x) \propto k_x^{\alpha} + \text{higher orders}. \tag{31}$$

Differentiating $\ln \omega$ yields for $k_x \to 0$

$$\alpha = \lim_{k_x \to 0} k_x \int_0^{x_0} \partial_{k_x} f(x; k_x)\, \mathrm{d}x. \tag{32}$$

We decompose P and Q in linear factors:

$$P(x; k_x) = (x - p_1(k_x))(x - p_2(k_x)) \cdots (x - p_M(k_x)) \tag{33}$$

$$Q(x; k_x) = (x - q_1(k_x))(x - q_2(k_x)) \cdots (x - q_N(k_x)) \tag{34}$$

such that $q_1(k_x)|_{k_x=0} = x_0$. In this way the factor $(x - q_1(k_x))$ dominates the behaviour of α for small k_x. Further, since the dispersion is invariant under the substitution $k_x \to -k_x$ we have A, p_i, $q_i \propto k_x^2$ for small k_x. Thus we are led to write $q_1(k_x) = x_0 + \beta k_x^2$, with positive β. With these preparations we rewrite equation (32):

$$\alpha = \lim_{k_x \to 0} k_x \int_0^{x_0} \frac{2\beta k_x}{(x \underbrace{-x_0 - \beta k_x^2}_{-q_1})^2} g(x; k_x)\, \mathrm{d}x \tag{35}$$

$$= \lim_{k_x \to 0} 2 \int_0^{x_0/(\beta k_x^2)} \frac{g(x_0 - \beta k_x^2; k_x)}{(1+y)^2}\, \mathrm{d}y \tag{36}$$

where we substituted $x = x_0 - \beta k_x^2 y$ and $g(x; \boldsymbol{k})$ for $A(k_x)P(x; k_x)(x - q_1)/Q(x; k_x)$. Taking the limit yields

$$\alpha = 2g(x_0; 0) \int_0^{\infty} \frac{1}{(1+y)^2}\, \mathrm{d}y = 2g(x_0; 0). \tag{37}$$

A straightforward calculation shows that

$$g(x_0; 0) = A(0) \frac{P(x_0; 0)}{\partial_x Q(x_0, 0)} \tag{38}$$

which we can easily calculate. Figure 7 shows the exponent α as function of the angle ϕ measured from the positive x-axis to the negative y-axis.

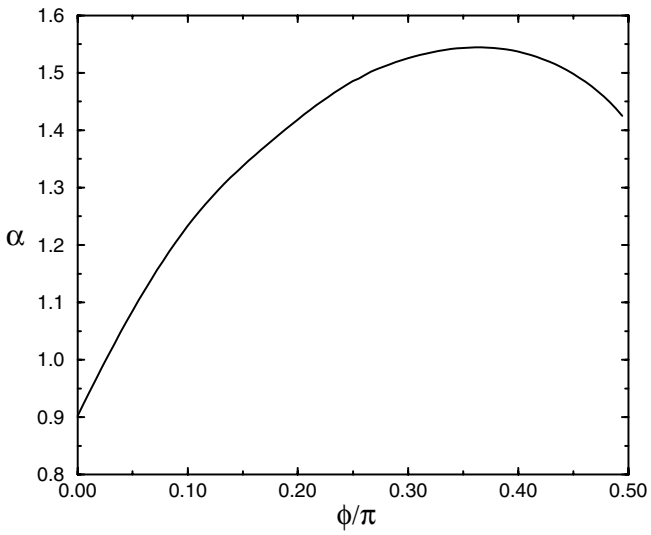

Figure 7. The exponent α in $\omega(k_x) \propto k_x^{\alpha}$ as a function of the angle ϕ between the x- and $-y$-axes.

There is only one ratio x/y for which $\alpha = 1$. At this point the dispersion vanishes with finite spin-wave velocity ($\phi \approx 0.081(1)$ or $x \approx 0.679(1)$, $y \approx -0.055(1)$).

Let us turn to a comparison of the theoretical dispersion to experimental data for $SrCu_2(BO_3)_2$. To fit the dispersion to the experimental data we make use of the parameter dependence of our results by requiring the curves to go through certain points and solve the resulting set of equations. At $\boldsymbol{k} = (0, 0)$, ESR [14], FIR [15] and INS [7] data suggest a value of $\omega(0, 0) = 2.98$ meV. At finite $\boldsymbol{k}$ we have to rely on the INS measurements, which contain

rather large errors. In figure 8 we show the INS data (bullets and error bars) and two of our fitted curves. For the parameter values given we get an excellent agreement.

Because of the flatness of the dispersion and the comparably large error bars, it is not possible to fix the model parameters unambiguously. As sketched in figure 8 one can lower x and enlarge J_1 and $|y|$ while maintaining reasonable agreement. On the basis of the one-triplet dispersion, it is not possible to fix the model parameters quantitatively. Our investigation in the two-triplet sector [8] (where y is disregarded, since it is probably not very important) enables us to fix the parameters to the intervals ($y = 0$) $x = 0.603(3)$ and $J_1 = 6.16(10)$ meV. The corresponding one-triplet dispersion is the solid curve in figure 8.

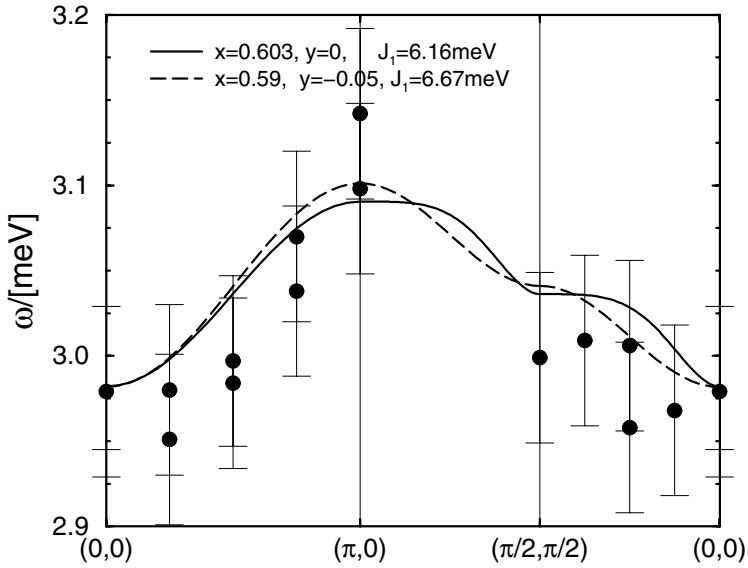

Figure 8. One-triplet dispersion. Our theoretical results fitted to INS data (bullets, errors at least as large as the error bars). Due to the large errors it is not possible to fit the model parameters unambiguously.

5. Conclusions

In summary, we have demonstrated the utility of our perturbation method introduced earlier [9]. By the means of a continuous unitary transformation, the original Hamiltonian is mapped onto a block diagonal, energy-quanta-conserving, effective Hamiltonian $\mathcal{H}_{\text{eff}}$. This allows to do the calculations for different energy sectors separately.

Here we used this method to develop a picture of excitation processes in a model for $SrCu_2(BO_3)_2$ and calculated the series expansion of the one-magnon dispersion ω about the limit of isolated dimers as a 15th-order polynomial in the model parameters.

We showed that the dispersion decomposes into two nearly degenerate branches with a splitting proportional to x^{10}. At $\boldsymbol{k} = \boldsymbol{0}$ and at the border of the magnetic Brillouin zone the two branches fall onto each other. By making use of our detailed analysis of the model symmetries we showed that point group operations alone cannot explain these degeneracies. In fact we showed that the model's space group symmetries have to be taken into account.

Moreover we analysed the critical behaviour of ω for small $|\boldsymbol{k}|$ at various ratios of x and y. It is found that the dispersion vanishes only for $x \approx 0.679(1)$ and $y \approx -0.055(1)$ with a

finite spin velocity.

Finally, we fitted our dispersion to INS data obtained by Kageyama *et al* [7] and found that it is not possible to fix the model parameters unambiguously from just the one-triplet data due to very large experimental error bars. The parameter values determined by our investigations in the two-triplet sector (reference [8]: $y = 0$, $x = 0.603$, $J = 6.67$ meV), however, lead to a one-magnon dispersion agreeing nicely with the experimental findings.

Acknowledgments

The authors would like to thank Alexander Bühler for helpful discussions and the Regional Computing Centre of the University of Cologne (RRZK) and Dr Kim Yong Taik in particular for generous assistance with our large-scale computations. This work was supported by the DFG-Schwerpunkt 1073 and by the SFB 341.

Appendix A

First we show that $\mathrm{d}t_r = 0$ if $r_1 = r_2$.

With equation (20) (the σ_v-symmetry) we have

$$t_{\boldsymbol{s}}^{o(\boldsymbol{r})} = t_{s_2,s_1}^{o(\boldsymbol{r}-(0,1))}. \tag{A.1}$$

Splitting both sides according to equation (14) we get

$$\bar{t_{\boldsymbol{s}}} + \mathrm{e}^{\mathrm{i}\boldsymbol{Q}\cdot\boldsymbol{r}}\,\mathrm{d}t_{\boldsymbol{s}} = \bar{t}_{s_2,s_1} + \mathrm{e}^{\mathrm{i}\boldsymbol{Q}\cdot(\boldsymbol{r}-(0,1))}\,\mathrm{d}t_{s_2,s_1} \tag{A.2}$$

leading to

$$\bar{t_{\boldsymbol{s}}} + \mathrm{d}t_{\boldsymbol{s}} = \bar{t}_{s_2,s_1} - \mathrm{d}t_{s_2,s_1} \qquad \text{for } r \text{ even} \tag{A.3}$$

$$\bar{t_{\boldsymbol{s}}} - \mathrm{d}t_{\boldsymbol{s}} = \bar{t}_{s_2,s_1} + \mathrm{d}t_{s_2,s_1} \qquad \text{for } r \text{ odd.} \tag{A.4}$$

Taking the difference of the two equations yields

$$\mathrm{d}t_{s_1,s_2} = -\mathrm{d}t_{s_2,s_1} \tag{A.5}$$

which proves the assertion. In particular $\mathrm{d}t_{\boldsymbol{0}} = 0$.

We now show that $\mathrm{d}t_r = 0$ if $r_1 + r_2$ is an odd number.

According to equation (13) we have

$$t_{\boldsymbol{r}'}^{o(\boldsymbol{r})} = \langle \boldsymbol{r}+\boldsymbol{r}'|\mathcal{H}_{\mathrm{eff}}|\boldsymbol{r}\rangle = \langle \boldsymbol{r}|\mathcal{H}_{\mathrm{eff}}|\boldsymbol{r}+\boldsymbol{r}'\rangle = t_{-\boldsymbol{r}'}^{o(\boldsymbol{r}+\boldsymbol{r}')} = t_{\boldsymbol{r}'}^{o(\boldsymbol{r}+\boldsymbol{r}')} \tag{A.6}$$

since $\mathcal{H}_{\mathrm{eff}}$ has only real matrix elements in this basis (cf. equation (3)). The last equality follows from equation (18). Splitting both sides according to equation (14) yields

$$\bar{t_{\boldsymbol{r}}'} + \mathrm{e}^{\mathrm{i}\boldsymbol{Q}\cdot\boldsymbol{r}}\mathrm{d}t_{\boldsymbol{r}}' = \bar{t_{\boldsymbol{r}'}} + \mathrm{e}^{\mathrm{i}\boldsymbol{Q}\cdot\boldsymbol{r}}\mathrm{e}^{\mathrm{i}\boldsymbol{Q}\cdot\boldsymbol{r}'}\,\mathrm{d}t_{\boldsymbol{r}}' \Rightarrow \mathrm{d}t_{\boldsymbol{r}}' = \mathrm{e}^{\mathrm{i}\boldsymbol{Q}\cdot\boldsymbol{r}'}\,\mathrm{d}t_{\boldsymbol{r}}' \Rightarrow \mathrm{d}t_{\boldsymbol{r}}' = 0 \qquad \text{for } r_1' + r_2' \text{ odd.} \tag{A.7}$$

Appendix B. Degeneracy of ω

The dispersion (29) will be twofold degenerate if the square root vanishes. We will use the shorthand $\boldsymbol{r}$ even/odd for $r_1 + r_2$ even/odd.

B.1. $\boldsymbol{k} = 0$

B.1.1. $b \stackrel{!}{=} 0$. For $\boldsymbol{k} = 0$ equation (28) gives

$$\frac{b}{2} = \sum_{\substack{r>0 \\ r \text{ even}}} \mathrm{d}t_r = \sum_{\substack{r_1=0 \\ r_2>0 \\ r \text{ even}}} \mathrm{d}t_r + \sum_{\substack{r_1>0 \\ r_2=0 \\ r \text{ even}}} \mathrm{d}t_r + \sum_{\substack{r_1>0 \\ r_2>0 \\ r \text{ even}}} \mathrm{d}t_r + \sum_{\substack{r_1>0 \\ r_2<0 \\ r \text{ even}}} \mathrm{d}t_r = I_1 + I_2 + I_3 + I_4. \tag{B.1}$$

We rewrite the first and the third sum on the right-hand side of equation (B.1):

$$I_1 = \sum_{\substack{r_1>0 \\ r_2=0 \\ r \text{ even}}} \mathrm{d}t_{-r_2,r_1} \qquad \text{and} \qquad I_3 = \sum_{\substack{r_1>0 \\ r_2<0 \\ r \text{ even}}} \mathrm{d}t_{-r_2,r_1}. \tag{B.2}$$

From equation (21) (the R-symmetry) we deduce

$$\mathrm{d}t_{r_1,r_2} = -\mathrm{d}t_{-r_2,r_1}$$

and see that $I_1 = -I_2$ and $I_3 = -I_4$. Hence we find $b = 0$.

B.1.2. $(a_0 - a_1) \stackrel{!}{=} 0$. For $\boldsymbol{k} = 0$ we have (cf. equation (27))

$$\frac{a_0 - a_1}{2} = \sum_{r>0} \bar{t}_r \left[1 - \cos(\pi(r_1 + r_2))\right] = 2 \sum_{\substack{r>0 \\ r \text{ odd}}} \bar{t}_r \tag{B.3}$$

and, recalling that $\mathrm{d}t_r = 0$ for r odd, equation (21) yields

$$\bar{t}_{r_1,r_2} = -\bar{t}_{-r_2,r_1} \tag{B.4}$$

so we can use the same splitting as in equation (B.1). Thus the energy degeneracy at $\boldsymbol{k} = 0$ is due to the rotational symmetry R as defined in section 3.

B.2. $k_x + k_y = \pi$

B.2.1. $b \stackrel{!}{=} 0$. Making use of $\mathrm{d}t_r = \mathrm{d}t_{-r}$, which follows from equation (18), we have for $k_y = \pi - k_x$

$$\frac{b}{4} = \sum_{\substack{r \\ r \text{ even}}} \mathrm{d}t_r \cos(k_x(r_1 - r_2) + \pi r_2) = \sum_{\substack{r_1,r_2 \\ r \text{ even}}} \mathrm{d}t_{r_2,r_1} \cos(k_x(r_2 - r_1)) \cos(\pi r_1). \tag{B.5}$$

In the last step we choose to rearrange the sum and observe that if r is even we have r_1 and r_2 both odd or both even. In both cases the identity

$$\cos(\pi r_1) = \cos(\pi r_2) \tag{B.6}$$

holds. Inserting relation (A.5) in the last row of equation (B.5) we end up with

$$\frac{b}{4} = -\sum_{\substack{r \\ r \text{ even}}} \mathrm{d}t_r \cos(k_x(r_1 - r_2)) \cos(\pi r_2) \tag{B.7}$$

resulting in $b = -b$ and thus $b = 0$.

B.2.2. $(a_0 - a_1) \stackrel{!}{=} 0$. Analogously to in subsection B.1.2, we have here

$$\begin{aligned}\frac{a_0 - a_1}{4} &= \sum_{\boldsymbol{r}} \bar{t}_{\boldsymbol{r}} \left[\cos(\boldsymbol{k}\cdot\boldsymbol{r}) - \cos(\boldsymbol{k}\cdot\boldsymbol{r} + \pi(r_1 + r_2))\right] = 2\sum_{\boldsymbol{r}\ \text{odd}} \bar{t}_{\boldsymbol{r}} \cos(k_x(r_1 - r_2) + \pi r_2) \\ &= 2\sum_{\boldsymbol{r}\ \text{odd}} \bar{t}_{r_2,r_1} \cos(k_x(r_2 - r_1))\cos(\pi r_1) \\ &= -2\sum_{\boldsymbol{r}\ \text{odd}} \bar{t}_{r_1,r_2} \cos(k_x(r_1 - r_2))\cos(\pi r_2) \qquad \text{(B.8)}\end{aligned}$$

where the last but one equality follows from equation (20) (the σ_v-symmetry), i.e. $\bar{t}_{r_1,r_2} = \bar{t}_{r_2,r_1}$, and from the fact that if $\boldsymbol{r}$ is odd we have that r_1 is odd and r_2 even or r_1 is even and r_2 odd. From that we see that $\cos(\pi r_1) = -\cos(\pi r_2)$.

The degeneracy over the remaining three borders of the magnetic Brillouin zone can be shown analogously. It is interesting to note that the calculations necessarily involved glide line operations. The degeneracies can thus not be explained by considering point group symmetries only.

References

[1] Taniguchi S *et al* 1995 *J. Phys. Soc. Japan* **64** 2758
[2] Garrett A W *et al* 1997 *Phys. Rev. Lett.* **79** 745
[3] Kageyama H *et al* 1999 *Phys. Rev. Lett.* **82** 3168
[4] Miyahara S and Ueda K 1999 *Phys. Rev. Lett.* **82** 3701
[5] Shastry B S and Sutherland B 1981 *Physica* B **108** 1069
[6] Müller-Hartmann E *et al* 2000 *Phys. Rev. Lett.* **84** 1808
[7] Kageyama H *et al* 2000 *Phys. Rev. Lett.* **84** 5876
[8] Knetter C, Bühler A, Müller-Hartmann E and Uhrig G S 2000 *Preprint* cond-mat/0005322
[9] Knetter C and Uhrig G S 2000 *Eur. Phys. J.* B **13** 209
[10] Miyahara S and Ueda K 2000 *Phys. Rev.* B **61** 3417
[11] Zheng Weihong, Hamer C and Oitmaa J 1999 *Phys. Rev.* B **60** 6608
[12] Domb C and Lebowitz J L (ed) 1983 *Phase Transitions and Critical Phenomena* vol 13 (London: Academic)
[13] Albrecht M and Mila F 1996 *Europhys. Lett.* **34** 145
[14] Nojiri H *et al* 1999 *J. Phys. Soc. Japan* **68** 2906
[15] Room T *et al* 2000 *Phys. Rev.* B **61** 14 342